Astron. Astrophys. 335, 449–462 (1998)

ASTRONOMY AND ASTROPHYSICS

Galactic models with massive coronae

V. The spiral Sab galaxy M 81

P. Tenjes[1,2], **U. Haud**[2], **and J. Einasto**[2]

[1] Institute of Theoretical Physics, Tartu University, Tähe 4, EE-2400 Tartu, Estonia
[2] Tartu Observatory, EE-2444 Tõravere, Estonia (tenjes@aai.ee, urmas@aai.ee, einasto@aai.ee)

Received 3 March 1998 / Accepted 20 April 1998

Abstract. Stellar populations in spiral galaxy M 81 are studied by using modelling. The galaxy is assumed to be stationary and consisting of a superposition of several subsystems. Each subsystem corresponds to a certain stellar/gas/dark matter population with a certain density distribution, chemical composition and kinematical characteristics. We presume that equidensity surfaces of the galactic populations are similar concentric ellipsoids or can be represented as sums of such ellipsoids. The input observational data base consists of surface photometry along the minor and major axis in UBVRI colours, rotation velocities of gas, stellar velocity dispersions, distribution and kinematics of globular clusters, distribution of the young stellar component and gas, kinematics of M 81 satellite galaxies. These data are used to decompose the galaxy into a central nucleus, a metal-rich core and a bulge, a metal-poor halo, an old stellar disk, a young gaseous-stellar disk and a massive dark matter component. Each population is characterized by its ellipticity, radius, mass, luminosity, structure parameter and colour indices. These population parameters are found using the least-squares algorithm. The algorithm minimizes the sum of squares of relative deviations of the model from observations. The values of the parameters were calculated in several steps from a preliminary crude model to the final model. The sensitivity of the population parameters to various observational data is analysed. Particular attention is devoted to the dark matter problem. In the final model the mean mass-to-luminosity ratio of the optically visible parts of the galaxy is found to be $M/L_{\rm B} = 5.4 \pm 2.4\,{\rm M}_\odot/{\rm L}_\odot$, and the ratio of the total mass to the visible one $M_{\rm T}/M_{\rm vis} = 44$. In the inner regions the best fit with observations is obtained when a central point mass $2.7 \cdot 10^8\,{\rm M}_\odot$ is added to the nucleus.

Key words: galaxies: spiral – galaxies: structure – galaxies: individual: M 81 – galaxies: nuclei – cosmology: dark matter

1. Introduction

To understand the evolution of galaxies quantitative information is needed for individual galactic populations. Traditionally dynamical models of galaxies are constructed with the aim to determine the overall mass distribution of galaxies. Yet galaxies consist of populations of different properties which also differ in their mass distribution. For this reason in most mass distribution models several populations are considered, most frequently the bulge and disk, and in recent models also a massive dark matter (DM) population (Kent 1987, Simien 1988, Shaw & Gilmore 1990, Prieto et al. 1992, de Jong 1996; for review see e.g. Capaccioli & Caon 1992). Only for our own Galaxy more detailed population structure is studied (see for example Gilmore et al. 1990, van der Kruit & Gilmore 1995, Ng et al. 1997, Méra et al. 1998).

A direct determination of parameters characterizing their structure is difficult as from observations it is possible to derive integrated properties of galaxies summed over all populations. To overcome this difficulty modelling of *galactic populations* is needed. This is not a trivial task. Principles of modelling galactic populations were elaborated by Einasto (1967a, 1967b, 1969a), and applied to determine population parameters for the Andromeda galaxy (Einasto 1969b, Einasto & Rümmel 1972) and Galaxy (Einasto 1969a, Einasto 1970, Einasto & Einasto 1972b). This study showed the presence of a mass paradox: photometric data indicate the end of the visible galaxy at a distance from galaxy center $\approx$ 20 kpc, whereas kinematic data suggest a much larger size of the galaxy. This mass paradox can be solved by adding a massive and large dark matter population to galactic models (Einasto 1972).

In these early models population parameters were determined by a trial-and-error procedure using graphs for galactic descriptive functions (Einasto & Einasto 1972a). Later Haud (1985) elaborated a method to determine population parameters by an automated computer algorithm. This method was described by Einasto & Haud (1989, Paper I) and applied to our Galaxy (Haud & Einasto 1989, Paper II), M 87 (Tenjes et al. 1991, Paper III), and M 31 (Tenjes et al. 1994, Paper IV).

In the present paper we investigate the structure of the nearby SA(s)ab galaxy M 81 and determine the parameters of its main stellar populations. We try to estimate the accuracy of these parameters and their sensitivity to a different kind of observational data. The decomposition of a galaxy into subsystems is complicated and often uncertain. Due to the large number of free parameters there may not be a unique solution to the problem.

Send offprint requests to: P. Tenjes (second address)

But when using large samples of observational data and comparing the values of the parameters during the modelling also with the models of chemical evolution it is possible to avoid obviously unphysical solutions. The uncertainty can be diminished by confining ourselves to well-observed galaxies. Its relatively large size in the sky makes the galaxy M 81 suitable for detailed studies of stellar content and for discrimination of stellar ensembles by their spatial distribution, chemical composition, kinematics and age.

M 81 is an example of galaxies with a falling rotation curve. In connection with this we have to answer a question, whether there is any dark matter associated with M 81. The two-component model consisting of a bulge and a disk calculated by Rohlfs & Kreitschmann (1980) included no DM. Also Kent (1987) has found that in his sample of 16 galaxies the galaxy M 81 may be the only one where, in addition to the luminous components, it is not necessary to include the DM component. Both these models are based on the surface photometry and on the rotation curve observations.

An additional and independent basis for mass determination is provided by the kinematics of the satellite galaxies surrounding M 81. In this case we need to decide what galaxies are gravitationally bound with M 81. Different samples of satellite galaxies may influence the quantitative mass estimates but the first glance at the highly different radial velocities of four neighbouring galaxies M 81, M 82, NGC 3077, and NGC 2976 hints that the problem of the existence of the DM component in M 81 is worth reconsideration.

The models taking into account the kinematics of satellite galaxies have been constructed by Einasto et al. (1980a, 1980b). However, the amount of different observational data has considerably increased, which made it necessary to review our earlier models.

Sect. 2 describes the observational data used in the modelling process. In Sect. 3 we characterize the subsystems in M 81: the nucleus, the metal-rich core, the bulge, the metal-poor halo, the old disk, the extreme flat subsystem, and the invisible massive corona, and emphasize which parameters were kept fixed during the final best-approximation fit for a particular subsystem. Sect. 4 and Appendix A are devoted to the modelling process. In Sect. 5 we give the parameters and mass distribution functions of our final model and in Sect. 6 the discussion of the model is presented.

Throughout this paper all luminosities and colour indices have been corrected for absorption in our Galaxy according to Burstein & Heiles (1984) and Freedman et al. (1994): A_B =0.14. The distance to M 81 has been taken 3.6 Mpc (Freedman et al. 1994), the position angle of the major axis PA = 150°, the angle of inclination to the line of sight i =32°(Garcia-Gomez & Athanassoula 1991).

2. Analysis of observational data

By now a detailed *surface photometry* of M 81 is available in UBVRI colours. Table 1 presents references, the faintest observed isophotes ($\mathrm{mag\ arcsec^{-2}}$), corresponding distances along the major axis ($'$) and colour system used. In addition, the surface brightness distribution of M 81 has been obtained by Simkin (1967) but it is difficult to convert the coordinate system used in this paper to the major or minor axis and we have not used these data.

Table 1. Photometrical data

Reference	Faintest isophote	Radius ($'$)	Colour system
Brandt et al. 1972	24.5	9.8	BV
Crane et al. 1993	16.6	0.08	V
Elmegreen & Elmegreen 1984	(25.3)	12.4	BI
Georgiev & Getov 1991	21.5	2.0	BV
Guidoni et al. 1981	(25.3)	13.1	UBVRI
Högner et al. 1971	24.6	10.8	UBV
Illingworth 1980	18.7	0.96	R
Markaryan et al. 1962	26.1	9.1	BV
Keel 1989	(16.6)	0.05	B
Kent 1987	22.5	7.1	R
Kormendy 1985	(17.2)	0.18	V
Sandage et al. 1969	21.1	1.2	UBV
Schweizer 1976	24.7	10.6	UBVR
Tenjes 1992	24.5	9.9	UB

The composite surface brightness profiles in the UBVRI colours along the major and minor axes were derived by averaging the results of different authors. Isophotes were well approximated by ellipses with different eccentricities. The observations for which the "Faintest isophote" value in Table 1 is in parenthesis were made without absolute calibration. They were calibrated with the help of other calibrated profiles in the same colour. For I-colour we have no absolute calibration and this profile entered our initial data set in arbitrary units. For this reason we do not have the I-colour luminosities of galactic populations in our final model. All the surface brightness profiles obtained in this way (in UBVRI along the major axis and in UBVR along the minor axis) belong to the initial data set of our model construction. Here we present the surface brightness distribution in V (Fig. 1), (B–V), (U–B), and (V–R) colour indices (Fig. 2), for which the absolute calibration is available, and the axial ratios (the ratio of the minor axis to the major axis of an isophote) (Fig. 3) as functions of the galactocentric distance.

The *rotation curve* we used for the modelling is based on gas velocities. For the inner 1.7 kpc of the galaxy the [NII], [SII] and Hα radial velocities were obtained and rotation curve was constructed by Goad (1976). The radial velocities of CO clumps obtained by Sage & Westphal (1991) give us information on the rotation law at the distances of $\mathrm{R} = 1.4 - 3.3$ kpc from the centre. High-resolution HI observations at 25″and 50″resolution by Rots (1975), Visser (1980) and 2′ resolution by Gottesman & Weliachew (1975) cover the region of $\mathrm{R} = 3.8 - 22$ kpc. The outer parts of M 81 were mapped in HI with a resolution of 9–10′ (~ 9 kpc) by Roberts & Rots (1973) and by Rohlfs & Kreitschmann (1980). Recently a comprehensive velocity map of M 81 and nearby regions was made with VLA. Adler &

Westphal (1996) mapped inner regions from 4 kpc to 20 kpc with angular resolution 12″, Yun et al. (1994) observed velocity field with lower angular resolution (1′) but mapped also outer regions. The averaged rotation velocities for a region $\mathrm{R} < 22$ kpc are given in Fig. 4 by open circles. For outer parts (distances of $\mathrm{R} \simeq 25$ – 30 kpc) Yun mentioned that the rotation curve becomes flat at the level of about 170 km/s (their Fig. 2). This is designated in Fig. 4 by open diamonds. Two outermost velocity measurements by Rohlfs & Kreitschmann (1980) are marked by filled diamonds. Beyond ~ 30 kpc the HI kinematics will be influenced by tidal effects from neighbouring NGC 3034 and NGC 3077 galaxies (Yun et al. 1994).

Line-of-sight *velocity dispersion* profile in good seeing conditions ($\mathrm{FWHM} \sim 0.6''$) for the central regions ($\mathrm{R} <$ 0.015 kpc) was obtained by Keel (1989). The innermost measured dispersion at 0.003 kpc is from HST observations with post-COSTAR FOS by Bower et al. (1996). In the intermediate distance interval (R = 0.02 – 1.6 kpc) dispersions have been measured by Illingworth (1980), Delisle & Hardy (1992), Carter & Jenkins (1993), and Bender et al. (1994). We averaged the dispersions at various distance intervals with weights depending on seeing conditions and velocity resolution and derived the dispersion curve presented in Fig. 5 by open circles. Mean dispersion value within inner 1″ 170 km/s in in good agreement with the McElroy (1995) calibration (his Table 4).

The observed distributions and kinematics of *individual objects* (satellite galaxies, globular clusters, young stars, gas etc.) which we have used for the modelling will be referred to and analysed in Sects. 3.3, 3.4 and 3.6.

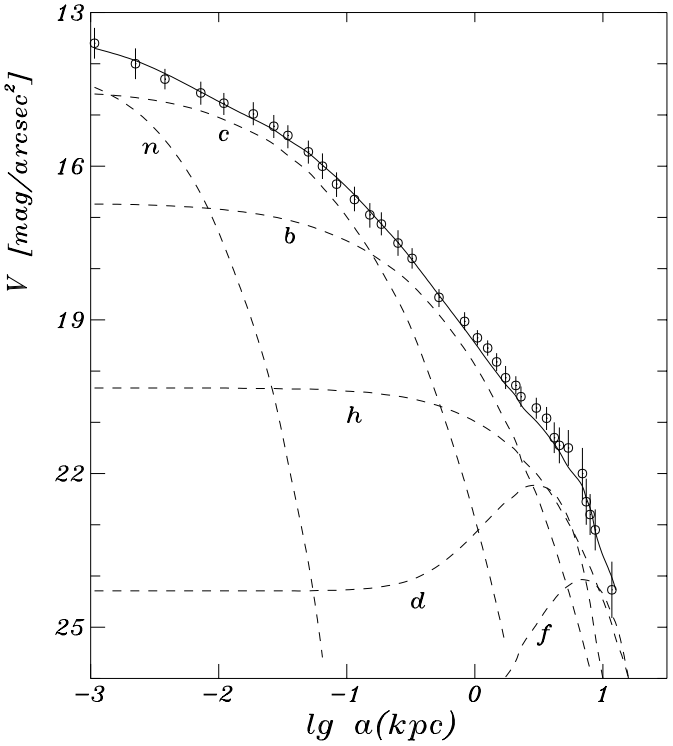

Fig. 1. The averaged surface brightness profile of M 81 in the V-colour. Open circles – observations, solid line – model, dashed lines – models for components (n – the nucleus, c – the core, b – the bulge, h – the halo, d – the disk, f – the extreme flat subsystem).

3. Subsystems in M 81

The general review of the stellar populations in our Galaxy can be found in textbooks by Mihalas & Binney (1981) and Gilmore et al. (1990) and in reviews by Hodge (1989), Majewski (1993). In the present section we describe the populations as they can be distinguished in external galaxies (cf. reviews by van den Bergh 1975, Hodge 1989) with special emphasis on M 81. For every population we emphasize what parameters of a subsystem are determined independently and thereafter kept fixed in the final best-approximation process.

3.1. The nucleus

Ho et al. (1996) divided the nucleus of M 81 into a narrow-line region and a broad-line region. In the narrow-line region they discriminated a lower density "halo" with a radius ~ 10 pc and denser "core" with a radius about 0.1–1 pc. For broad-line region crude estimates gave the radius $\sim 0.001 - 0.004$ pc. The mass of broad-line region was estimated to be $M \sim (0.7-3) \cdot 10^6\,\mathrm{M}_\odot$. According to Bower et al. (1996) the broad-line component originates most likely from the elliptical accretion disk. This interpretation is consistent with HST Hα image of the nucleus obtained by Devereux et al. (1997) and with VLBI observations by Bietenholz et al. (1996). Thus we suppose the broad-line region to be a gas disk surrounding a point mass (black hole). Further we will neglect the gas disk mass and take into account only the black hole (BH) mass.

Now we may estimate the mass of the larger stellar component (narrow-line region) which we call here the nucleus. One constraint is the stellar velocity dispersion 250 km/s measured by Bower et al (1996) using the HST FOS camera at the galactocentric distance $r = 0.15'' = 2.6$ pc. We take this value as the mean line-of-sight velocity dispersion of the nucleus. The radius of the nucleus as well as the structure parameter and the luminosity is derived from the surface photometry of the central regions of M 81. The surface photometry of the nuclear region with the highest angular resolution is done by Crane et al. (1993) with HST FOC (f/96). From his photometric profile we obtain for the radius of the nucleus $a_0 = 6 \pm 2$ pc, the luminosity $L_V = (7.0 \pm 0.6) \cdot 10^6\,\mathrm{L}_\odot$ and structure parameter $N = 2.0 \pm 0.5$. With sufficient precision the nucleus can be taken as spherical (i.e. axial ratio $\epsilon = 1.$).

The mass of the nucleus was determined using formula (8) of the Appendix. For $M_{BH} = 3 \cdot 10^6\,\mathrm{M}_\odot$ this relation gives $M_{nucl} = 7.8 \cdot 10^8\,\mathrm{M}_\odot$ and $M/L_V = 110\,\mathrm{M}_\odot/\mathrm{L}_\odot$. This mass-to-light ratio is obviously too large for any stellar population. For this reason we study also a model where the M/L ratio of the nucleus was taken as an upper limit for an old metal-rich population (Bressan et al. 1994, Worthey 1994) $M/L_V = 11\,\mathrm{M}_\odot/\mathrm{L}_\odot$, giving $M_{nucl} = 7.5 \cdot 10^7\,\mathrm{M}_\odot$ and hence $M_{BH} = 2.65 \cdot 10^8\,\mathrm{M}_\odot$.

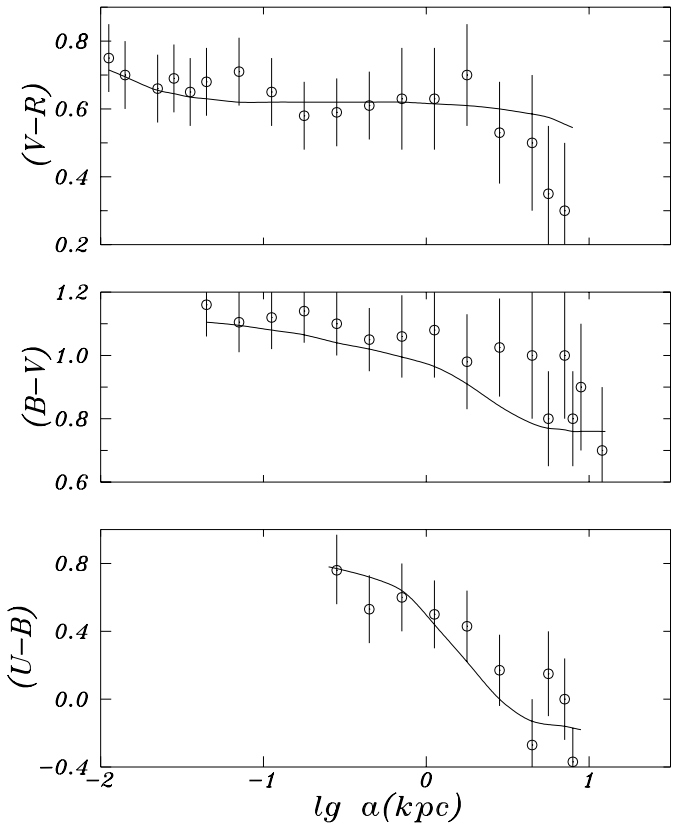

Fig. 2. The averaged profiles of the colour indices $(\mathrm{B}-\mathrm{V})$, $(\mathrm{U}-\mathrm{B})$ and $(\mathrm{V}-\mathrm{R})$ of M 81. Open circles – observations, solid line – model.

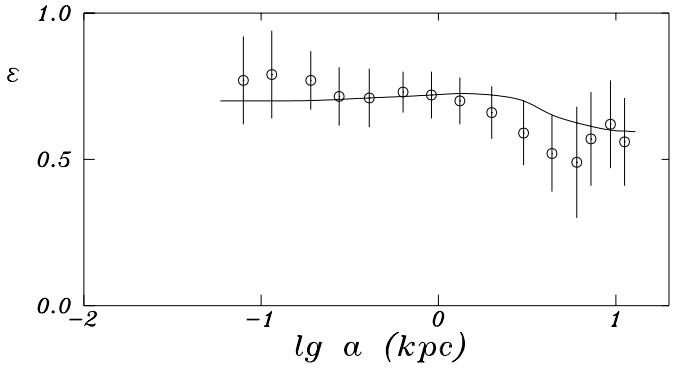

Fig. 3. The axial ratios of M 81 isophotes as a function of the galactocentric distance. Open circles – observations, solid line – model.

Although the nucleus is a prominent structural feature in galaxies, dynamically it is quite independent of the remaining subsystems. Thus we keep the parameters a_0, N, ϵ, L_V, M/L_V of the nucleus fixed during the final approximation procedure. More detailed structure of the nucleus and a central point source is beyond the scope of the present paper.

3.2. The core and the bulge

In general, the spheroidal parts of galaxies are not physically homogeneous (Rose 1985, Morrison & Harding 1993).

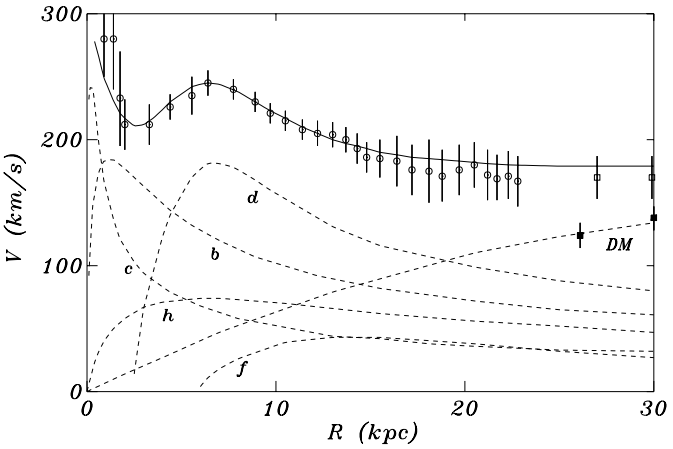

Fig. 4. The rotation curve of M 81. Open circles – high resolution observations of HI, ionized gas and CO, open squares – Yun et al. (1994), filled squares – Rohlfs & Kreitschmann (1980). Thick curve – our best-fit model, dashed curve – models for components (DM – dark matter).

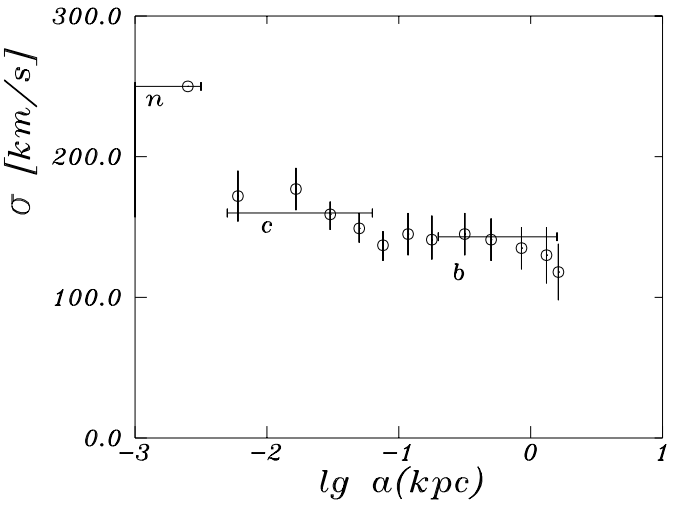

Fig. 5. The averaged line-of-sight velocity dispersion profile of M 81. Open circles – observed stellar dispersions, horizontal bars denote the mean dispersions calculated from our best fit model for the nucleus, the core and the bulge at the corresponding distance intervals.

It is convenient to define *the bulge* consisting of stars with normal (solar) metal content. This is one of the most prominent structural features of galaxies. In several nearby galaxies, in the inner regions of spheroids, a sudden increase in metallicity (Cohen 1979, Delisle & Hardy 1992, O'Connell et al. 1992, Davidge 1997) has been detected. In the case of M 81 this kind of increase was most strong inward of 0.3–0.5 kpc. Thus we separate a metal-rich *core* from the bulge.

The problem of discriminating between the core and the bulge is a complicated one and will be discussed in Sect. 4.2. All the parameters of the core and the bulge have been determined during the final approximation process.

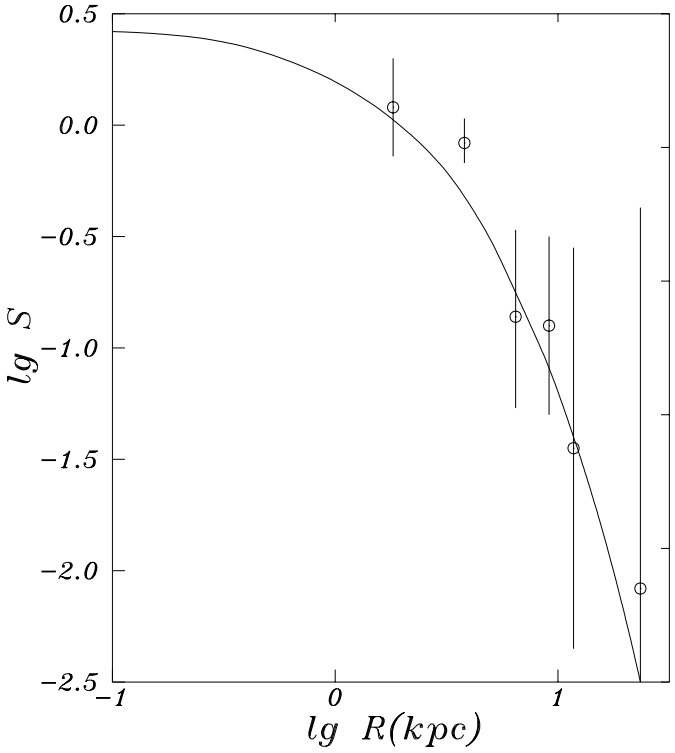

Fig. 6. The distribution of globular clusters in M 81. The observations by Perelmuter & Racine (1995) are presented by open circles. The continuous line gives our best-fit model distribution for the halo.

3.3. The halo

By 'halo' we mean a spheroidal metal-poor population II subsystem, typical representatives of which are old stars (like RR-Lyrae variables) and low metallicity globular clusters (GC). In M 81 there are no observations on the distribution of old star populations at present. Hence we must confine ourselves to the observations of GC.

The first effort to compile a sample of GC was made by Georgiev et al. (1991a, 1991b) on the basis of 6m (Russia) and 2m (Bulgaria) telescope plates. They estimated also B–V colour indices. However, in the present study we do not use their observations, because, as it was mentioned by the authors, the mean (B–V) colour of their sample is nearly $\sim 0.3^m$ redder than it could be expected. Taking into account quite moderate seeing $1.5 - 2''$ this sample may contain distant galaxies.

We use the sample of GC candidates selected by Perelmuter & Racine (1995) from CFHT plates and Mayall 4m telescope CCD frames. Resulting surface density distribution of GC candidates is given in Fig. 6 by open circles.

We estimated the flatness of GC subsystem from their Fig. 17 and found that the apparent axial ratio is ~ 0.7 giving us the true axial ratio $\epsilon = 0.55 \pm 0.15$. Thus the GC system in M 81 is not very spherical (the same holds also for galaxies M 87 and M 31 modelled by us earlier (Papers III and IV)).

Only old metal-poor GCs can be considered as test particles of the halo subsystem. Metallicity gradient of GC in Perelmuter & Racine's sample is weak with an exception of the innermost point at $R \sim 1.2$ kpc, thus we may conclude that in outer regions the contribution of bulge clusters is weak. In addition, the metallicity distribution of M 81 GC does not exhibit two-peaked distribution as is observed in some other galaxies (see Secker et al. 1995, Zepf et al. 1995, Elson & Santiago 1996) and their mean $(\mathrm{B-V}) \sim 0.7$ nearly coincides with the M31 halo cluster sample (Racine 1991, Reed et al. 1994). Thus we can expect that with possible exception of innermost clusters the Perelmuter & Racine's GC sample can be used as test particles of the halo subsystem.

The observed cluster distribution is well approximated by our density distribution law (Appendix, Eq. 1) with the parameters $N = 1.9 \pm 0.6$ and $a_0 = 4.5 \pm 0.5$ kpc. The mean colour indices for the M 81 cluster population are $(\mathrm{B-V}) = 0.70 \pm 0.05$, $(\mathrm{V-R}) = 0.46 \pm 0.04$.

For the mean velocity dispersion of GC population Perelmuter et al. (1995) derived 152 km/s. We use this value also in our model as an input parameter. Although this value is the halo object's dispersion, it is not determined by the halo mass only. GCs do not form even an approximately dynamically independent subsystem but lie in the gravitation field of the whole galaxy. Very important are the contributions due to disk and dark matter corona masses. Hence, in order to use the GC mean velocity dispersion the virial theorem for multicomponent systems must be used (Paper IV, App. A, Eq. (A8)).

As an independent value, related to mass, we use the mass-to-light ratio of GCs. According to the models by Pryor & Meylan (1993) the mean M/L ratio of GC in our Galaxy is $M/L_V = 2.3 \pm 1.1\ \mathrm{M_\odot/L_\odot}$. We take this value as a reasonable first approximation also for M 81 halo.

These values of the referred above GC population parameters (ϵ, N, a_0, M/L_V, $(B-V)$, $(V-R)$) are taken as fixed halo parameters in the final approximation process.

3.4. The extreme flat subsystem

Young stars and gas contribute most to the flat subsystem. The HI surface density distribution from observations made by Gottesman & Weliachew (1975) and Rots (1975) were converted to units $\mathrm{M_\odot/pc^2}$, reduced to total HI mass $M_{\mathrm{HI}} = 3.0 \cdot 10^9\,\mathrm{M_\odot}$ (Appleton et al. 1981, Yun et al. 1994) and averaged. The $\mathrm{H_2}$ surface densities from observations by Brouillet et al. (1988, 1991) and Sage & Westphal (1991) were converted also to units $\mathrm{M_\odot/pc^2}$ and averaged.[1] Composed in this way $\mathrm{H_2}$ surface density distribution gives the total $\mathrm{H_2}$ mass $M_{\mathrm{H_2}} = (1.0 \pm 0.3) \cdot 10^9\,\mathrm{M_\odot}$. (Outside ~ 9 kpc no $\mathrm{H_2}$ measurements are available. We extrapolated the data to this region. Corresponding additional uncertainties were included in the total mass error.) Thereafter the HI and $\mathrm{H_2}$ surface densities were added. The resulting surface density distribution of the gas is given in Fig. 7 by filled circles. The total gas mass is $M_{\mathrm{gas}} = (4.0 \pm 0.7) \cdot 10^9\,\mathrm{M_\odot}$.

[1] In $\mathrm{H_2}$ analysis Brouillet et al. assumed that CO emission is a realistic $\mathrm{H_2}$ tracer. In a recent study Allen et al. (1997) noted that this assumption may be incorrect and thus $\mathrm{H_2}$ mass is underestimated. Due

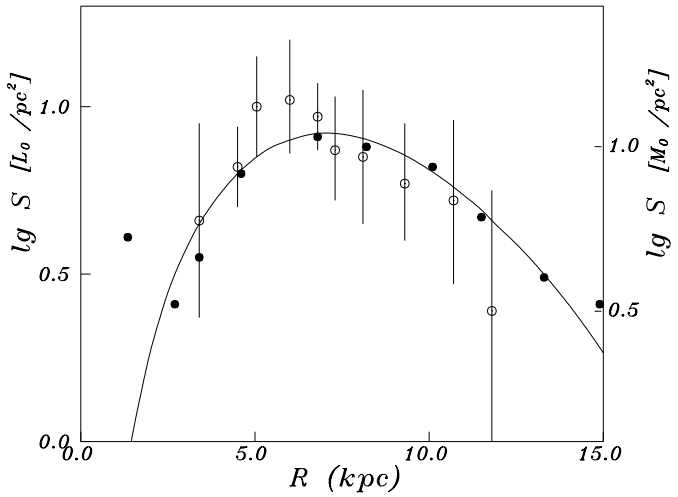

Fig. 7. The surface density distribution of the flat subsystem. Open circles and vertical scale units on the left-hand side – stellar component, filled circles and units on the right-hand side – gas component, solid curve – best-fit model distribution.

To obtain the stellar component distribution, we used the surface brightness distribution of spiral arms (Schweizer 1976), observations of OB-associations (Ivanov 1992) and HII regions (Hodge & Kennicutt 1983, Petit et al. 1988). The distributions of OB-associations and HII regions were deprojected "face on" and the number surface densities in concentric rings were calculated. Thereafter the distribution of surface brightness of spiral arms, the number surface density distribution of OB associations and HII regions were averaged. Resulting stellar component distribution is given in Fig. 7 by open circles (the vertical scale corresponds to the Schweizer's B-colour surface brightness measurements of spiral arms).

The total mass of young stars is derived by using the empirical Schmidt star formation law. If the power in the Schmidt law is $\alpha = 1$ the characteristic star formation time is $t_0 = 4.8$ Gyr and the present star formation rate in M 81 is $0.72\,\mathrm{M}_\odot/\mathrm{yr}$. If $\alpha = 2$ then $t_0 = 0.6$ Gyr and SFR = $0.21\,\mathrm{M}_\odot/\mathrm{yr}$ (this value is more consistent with SFR = $0.13\,\mathrm{M}_\odot/\mathrm{yr}$ determined by Hill et al. (1995) from UV emission). The mean of these two values gives the mass of stars with ages less than 1 Gyr $M_{\mathrm{stars}} = (0.6 \pm 0.3) \cdot 10^9\,\mathrm{M}_\odot$.

Therefore, the total mass of the flat subsystem of M 81 is $M = M_{\mathrm{gas}} + M_{\mathrm{stars}} = (4.6 \pm 0.8) \cdot 10^9\,\mathrm{M}_\odot$. The distribution of stars and gas of this population (Fig. 7) is well represented by the density distribution law (1) (see Appendix) with parameters $a_o = 8.3 \pm 0.7$ kpc, $N = 0.52 \pm 0.09$, $\kappa = 0.6 \pm 0.1$, $L_B = (2.3 \pm 0.7) \cdot 10^9\,\mathrm{L}_\odot$. For the flattening of the subsystem we take as in our Galaxy ϵ =0.02, for colour indices we take the values derived by Schweizer (1976) $(\mathrm{B} - \mathrm{V}) = 0.74$, $(U - B) = -0.17$, $(V - R) = 0.76$.

These values will be used in the least-square fit as fixed parameters for the flat subsystem.

to the lack of quantitative results we confined ourselves to the conventional $\mathrm{CO} \rightarrow \mathrm{H}_2$ conversion.

3.5. The disk

It is convenient to define the disk as consisting of stars with normal metallicity but with quite different ages (the mean age is about $7{\cdot}10^9\,\mathrm{yrs}$). As for the flat subsystem, we allow a toroidal structure for the disk, i.e. central density minimum. Otherwise it is difficult to model a minimum of the rotation velocity at 1 kpc (Einasto et al. 1980a; Rohlfs & Kreitschmann 1980). In determining the disk mass we do not assume the "maximum disk". Therefore we do not fix the disk parameters first. The problem of discrimination between the disk mass and possible dark matter amount in our model will be discussed in Sect. 4.3.

In the Milky Way there is probably, in addition to an ordinary old disk, an additional thick disk (e.g. Gilmore et al. 1995). As an hypothesis, this gives a sufficient reason to study the possible existence of a thick disk in M 81. Unfortunately, during the preliminary model construction we found that due to inclination of M 81 ($i = 32\,\mathrm{deg}$) the model is insensitive to analyse the vertical structure of the disk in detail. For this reason, we did not include a thick disk component in further modelling.

3.6. The massive corona

On the basis of very different observations it can be concluded that masses of galaxies are larger than it follows from a simple assumption of constant mass-to-light ratio. Large masses in the outer parts of galaxies result from the rotation velocities remaining constant at large galactocentric distances (Freeman 1993), from the thermal emission of hot gas detected in X-rays (Fabbiano 1989), from gravitational lensing effects (Blandford & Narayan 1992, Fort & Mellier 1994) etc. In the case of M 81 the mass distribution at largest distances is determined from the kinematics and distribution of M 81 satellite galaxies. We assume the corona to be spherical ($\epsilon = 1$).

To decide what galaxies form a bound group is not easy even when radial velocities of satellite galaxies are known (e.g. discussion in Huchtmeier & Skillman 1995). In our modelling we used the sample of 17 satellite galaxies with measured radial velocities from the study by van Driel et al. (1998) who gave the mean velocity dispersion of M 81 group $\langle\sigma\rangle = 114$ km/s. We approximated cumulative satellite spatial distribution with the density distribution formula (2) (see Appendix) with parameters $a_0 = 120 \pm 25$ kpc, $a^0/a_0 = 4.8 \pm 1.1$. Although the formal error in a^0/a_0 is not big, in reality it is coupled with the disk mass, allowing a wide range of possible disk masses. We will study the coupling of disk mass and the corona parameters in Sect. 4.3.

4. Best-approximation process

The stellar populations and mass distribution in M 81 have been studied by means of modelling. For all models the best-approximation parameter set has been found using the least-squares algorithm. The algorithm minimizes the sum of squares of relative deviations of the model from all observations.

The basic formulae and general steps of model construction were described in a previous paper (Tenjes et al. 1994) where the

stellar populations in the Andromeda galaxy were studied. In addition, the basic formulae in a compact form will be given in Appendix. Due to the nonlinear nature of these relations and the composite structure of the galaxies, fitting of the model to observations is not a straightforward procedure, and mathematically correct solution may be completely unphysical. (For example, a six-component model, where photometrical profile is approximated by some appropriate three components with nearly zero M/L ratios and rotational curve by other three components with very large M/L ratios may have nice fit with observations, but it is unphysical.) For this reason, the approximation process must be done in several steps.

First, the number of model components was fixed. The components we decided to include were described and emphasized in Sect. 3.

For three components – the nucleus, the extreme flat subsystem and the metal-poor halo subsystem – several parameters were determined independently of other subsystems (Sects. 3.1, 3.3, 3.4). In subsequent fitting processes they were kept fixed. This step allows to reduce the number of free parameters in the approximation process.

In the next stage crude estimates for remaining population parameters were made. The purpose of this step is only to exclude obviously unphysical values of parameters. During this stage we studied also the sensitivity of population parameters to different observations.

In the last stage the final model was constructed by the subsequent least-square approximation process.

4.1. Parameters of the approximation process

The set of initial data in final approximation process consists of:

1. photometrical data (surface photometry in UBVR colours along the major and minor axes, in I colour along the major axis);
2. the rotational curve in the plane of the galaxy;
3. the mean line-of-sight stellar velocity dispersion for the nucleus, the core and the bulge;
4. the mean line-of-sight velocity dispersion of globular clusters and satellite galaxies of M 81.

The total number of combined observational data points was 258, 216 data points of them are the surface brightness data, 39 data points describe the rotation curve and 3 points are the mean velocity dispersions of components. We assume that the rotation curve has the same total weight as the surface photometry. Thus, because the number of rotation data points is smaller than the number of photometry data points, the weight ascribed to each of them was correspondingly larger. The velocity dispersions were used only for mass determination.

In principle, in the seven-component model the maximum number of the degrees of freedom in the fitting process is 58 (6 visible populations with 9 parameters each (ϵ, a_o, M, κ, N, and 4 mass-to-light ratios in UBVR) and an invisible corona with 4 parameters (ϵ, a_o, a^0, M)). Some of these parameters can be fixed earlier. First, the parameter κ, indicating the depth of the central density depression, was taken zero for all components except the disk and the flat component. Further, the parameters of the nucleus were determined independently of others and fixed thereafter (Sect. 3.1). In Sect. 3.3 we derived the density distribution parameters ϵ, a_o, N, the colour indices (B–V), (V–R) and the mass-to-light ratio $M/L_{\rm V}$ of the halo from the distribution of globular clusters. In Sect. 3.4 from the distribution of the young stellar component all the parameters for the flat population were derived. These parameters of the halo and the flat subsystems were also unchanged. The parameters a_0, a^0, and ϵ of the corona were also fixed earlier (Sect. 3.6). When taking into account all the fixed parameters the number of free parameters is 28.

During the preliminary model construction the space of the remaining 28 parameters was divided into separate regions and analysed separately. The axial ratios of all subsystems form a nearly independent subspace, as they depend mainly on the light distribution along the minor axis, i.e. the projected isophotal eccentricities. Also the colour indices form an independent subspace, reducing the number of parameters to 15. Further, the masses and the luminosities of several subsystems depend also on different sets of observations. As it was in the case of modelling of the galaxy M 31 (paper IV), the most mixed are only seven parameters: the radii and the structure parameters of the core, the bulge and the disk, and the central depression of the disk. Coupling of these parameters is the most controversial part of the modelling process. We will analyse these problems in the following subsection.

4.2. Coupling of parameters

The core and the bulge subsystems are mixed in photometry, i.e. light profiles allow variation of their structural parameters in a quite large interval. When limiting to the light profile in V only and neglecting kinematics, the presence of the core is not even necessary. More strict limits to the parameters of these components result from kinematics: specific first maximum at about $R \simeq 1$ kpc and minimum at about $R \simeq 2$–3 kpc. To represent adequately both the inner part of the rotation curve and the surface photometry, a two-component inner spheroid with different M/L ratios is needed. From Fig. 8 it is seen that the model with the bulge component only and giving best fit with the rotation curve and surface photometry cannot be handled as a good one. Main characteristics of the inner parts of the rotation curve and surface brightness distribution are poorly fitted. Hence, further we study core + bulge models. From the modelling of the Milky Way rotation velocities Rohlfs & Kreitschmann (1988) also concluded that the bulge alone does not give the first maximum in the rotation curve and hence an additional inner component was needed.

In Fig. 9 we demonstrate the sensitivity of the rotation curve and the surface brightness distribution to the core radius. In these calculations the structure parameter N =3 and the mass of the core corresponds to the mean velocity dispersion of $\langle\sigma_{\rm core}\rangle$ =160 km/s. The radii of the core are 0.07, 0.14, and

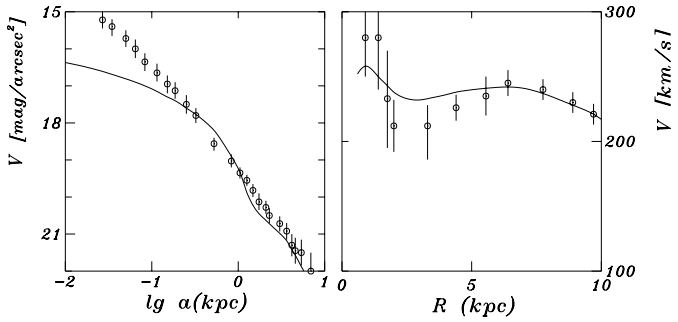

Fig. 8. The inner part of the rotation curve and the surface brightness distribution in V (cf. Figs. 1 and 4) for the best fit model without the inner metal-rich core. The mean calculated line-of-sight velocity dispersion for the bulge was fixed to be 145 km/s.

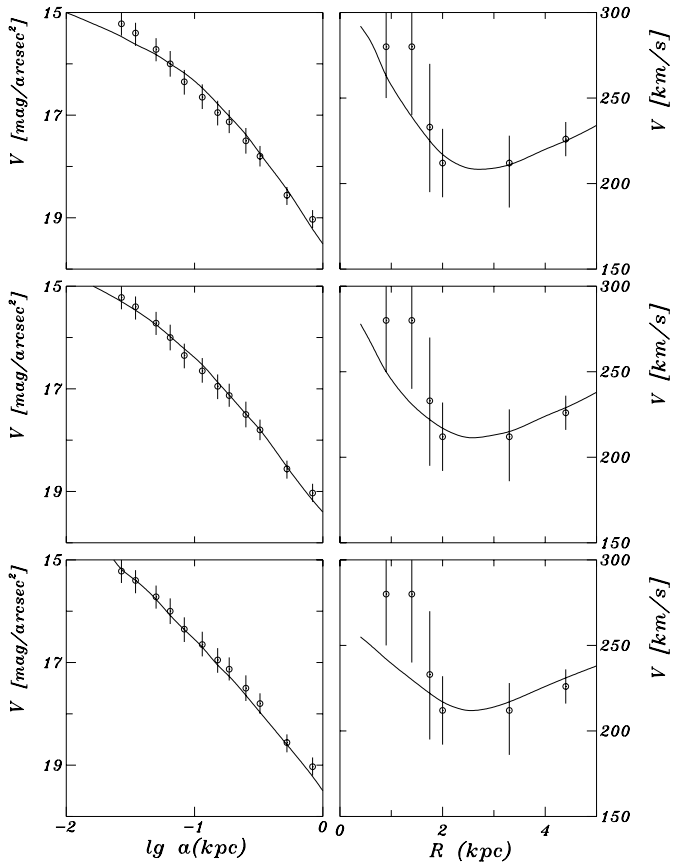

Fig. 9. The inner part of the rotation curve and the surface brightness distribution in V (cf. Fig. 1) for three different models. The core radii are 0.07 kpc, 0.14 kpc, 0.30 kpc for the lower, middle and upper panels, respectively.

0.30 kpc, the masses of the core are 0.3, 0.6, and 1.0 (in units of $10^{10}\,\mathrm{M}_\odot$) for models (a), (b), and (c), respectively. Fig. 10 illustrates models with a different structure parameter N of the core ($M = 0.35$, a_o =0.14 kpc). In model (a) N =1.5 and in model (b) N =5. As the radius of the core is more than seven times smaller than the radius of the bulge, the latter is quite insensitive to the changes of the core parameters and also to the parameters of all other components.

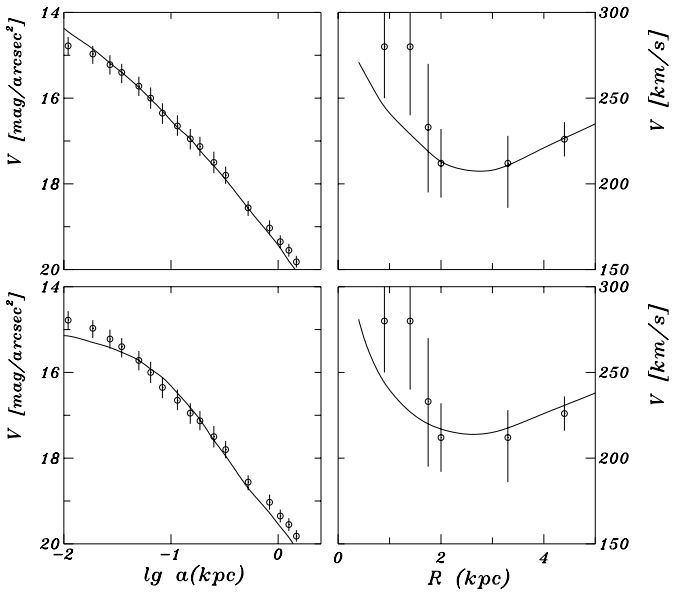

Fig. 10. The inner part of the rotation curve and the surface brightness distribution in V for two core models. In lower model N =1.5, in upper model N =5.

Since a_o and N for the halo parameters were fixed on the basis of the distribution of globular clusters, all the remaining parameters for the core and the halo, and all parameters for the bulge can be determined with sufficient accuracy.

4.3. The disk and the massive corona

The parameters of the disk depend both on photometrical and kinematical data. Increasing eccentricity of the isophotes beyond R >2 kpc (Fig. 3) indicates roughly the region where the disk becomes dominating in the photometry. In addition, the specific second maximum at R = 6.5 kpc in the rotation curve quite firmly determines the disk radius and the structure parameter N.

Fig. 11 illustrates the sensitivity of the rotation curve and the major axis brightness profile to the disk parameter κ. Models (a) and (b) correspond to the models with fixed parameters of the central depression κ =0.2 and κ =0.9, respectively. The radii of the disk were a_o =3.7 kpc and 4.2 kpc, the mass-to-light ratios 12 and 24 in B. In the case of κ =0.2 also the bulge mass decreases to $2.1\,\mathrm{M}_\odot$.

As we mentioned in Sect. 3.6 from observations the parameter of the corona a^0/a_0 is quite uncertain. This means also that the central density of the corona may vary considerably causing variation of the disk mass. Hence we must study the coupling of disk mass and dark matter density. In Fig. 12 two models for different disk masses are given. Model (a) has $M_d^+ = 5.7$, model (b) has M_d^+ =11.3. Other parameters of the disk as well as the radius of the corona were fixed. In both models the velocity dispersion of the corona was 114 km/s. It can be seen that in the case of M 81 the rotation curve allows quite firmly to discriminate between the visible and dark matter.

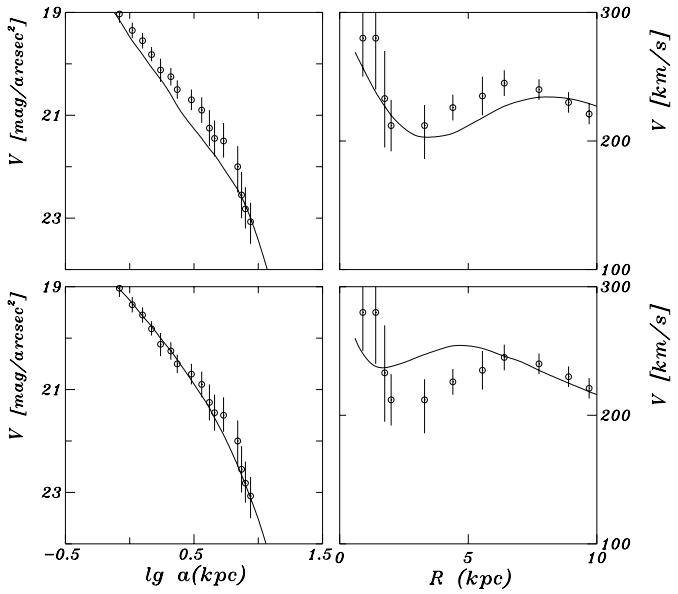

Fig. 11. The rotation curve and brightness profile for different central depression of the disk. In lower model κ =0.2, in upper model κ =0.9.

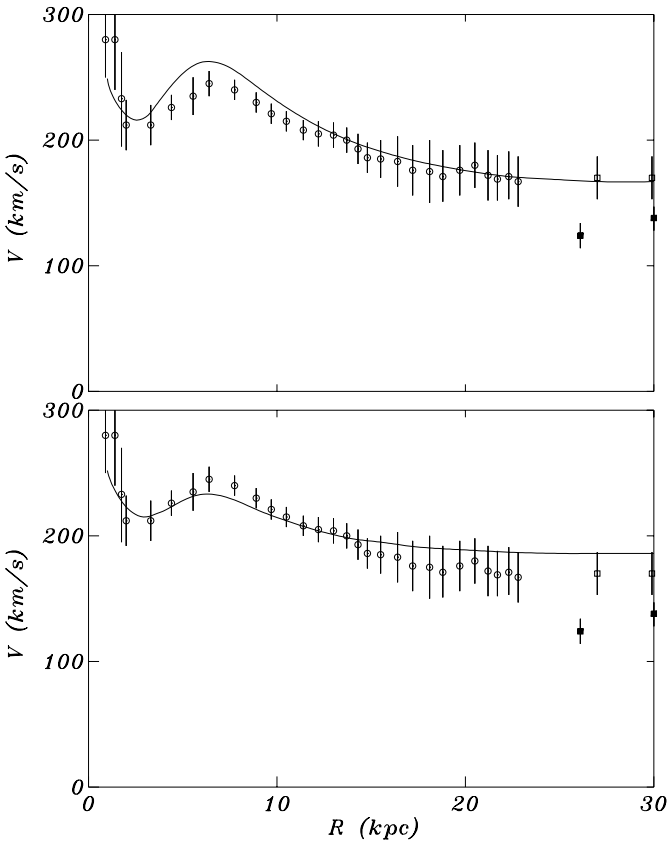

Fig. 12. The rotation curve of M 81 for different disk masses. In lower model $M_d^+ = 5.7$, in upper model $M_d^+ = 11.3$ (in units of $10^{10}\,\mathrm{M}_\odot$).

5. Results

The final seven-component model fits all photometric profiles with a mean relative error 0.7 per cent, and the rotation curve from $R = 2$ kpc to $R = 24$ kpc with the relative error 2 per cent. Therefore, the model is in good agreement with both data sets. The model describes well also the velocity dispersion data, the distribution of globular clusters and young stars + gas. The parameters of the final model (the axial ratio, ϵ, the harmonic mean radius, a_o, the total mass of the population, M, the structural parameters, κ and N, and the dimensionless normalizing constants, h and k, B-luminosities and colour indices) are given in Table 3, a colon designates fixed parameters. The final model is represented by solid lines in Figs. 1–7.

The total luminosity of M 81 is calculated to be $L_\mathrm{B} = (1.8 \pm 0.3) \cdot 10^{10}\,\mathrm{L}_\odot$, the optically visible mass $M_\mathrm{vis} = (9.7 \pm 2.6) \cdot 10^{10}\,\mathrm{M}_\odot$, the corresponding M/L ratio $5.4 \pm 2.4\,\mathrm{M}_\odot/\mathrm{L}_\odot$. The mass-to-light ratio of both disk-like components (disk + flat) together is $M/L_\mathrm{B} = 9.1\,\mathrm{M}_\odot/\mathrm{L}_\odot$, of all spheroidal components (nucleus+core+bulge+halo) together $M/L_\mathrm{B} = 3.9\,\mathrm{M}_\odot/\mathrm{L}_\odot$. Total luminosity of the spheroid is $L_B = 1.3 \cdot 10^{10}\,\mathrm{L}_\odot$.

Table 4 presents some descriptive functions calculated for our final model. $K_R \equiv \partial\Phi/\partial R$, where Φ is the gravitational potential, is the gradient of the gravitational potential in the radial direction (in the units of $\mathrm{km^2 s^{-2} kpc^{-1}}$) . $M(R)$ is the effective inner mass, defined as a point mass in the centre of the galaxy, having the same gravitational attraction at R as the subsystem. The quantity f_B is the local M/L ratio in the B-colour derived by dividing the effective mass and the effective luminosity in a shell limited by the radii R and $R + \Delta R$. The radii are in kiloparsecs, the masses in units of $10^{10}\,\mathrm{M}_\odot$, the M/L ratios in solar units.

The calculated local mass-to-luminosity ratios are given in Fig. 13. A clear difference between the visible and dark matter begins at the distance $R = 11$ kpc.

The mass-to-light ratio within the Holmberg radius $R =$ 19 kpc is $8.3\,\mathrm{M}_\odot/\mathrm{L}_\odot$. The radius at which the masses of dark matter and visible matter become equal is 26 kpc. These numbers indicate that the DM concentration around M 81 is significantly smaller than around M 31. However, because the extent of DM is larger than for M 31 the ratio of the total mass and visible mass M_T/M_{vis} is in both cases nearly the same ($M_T/M_{vis} = 44$ for M 81).

6. Discussion

The model of stellar populations constructed in this paper for the galaxy M 81 is based on a large body of observational data. Surface photometry along the major and minor axis in the UBVRI colours, rotation velocities, line-of-sight velocity dispersion data, distributions of gas and young stars, distribution and kinematics of globular clusters and satellite galaxies have been taken into account for decomposing the galaxy into subsystems and for the determination of population parameters.

On the basis of a smaller set of observational data several models were constructed earlier.

Monnet & Simien (1977) constructed a two-component model for M 81 ($r^{1/4}$ bulge + exponential disk) on the basis

Table 2. Model parameters

Population	a_0 (kpc)	M (10^{10} $M_\odot$)	ϵ	N	κ	h	k	M/L_B ($M_\odot/L_\odot$)	B-V	U-B	V-R
Nucleus	:0.006	:0.0075[a]	:1.	:2.	—	33.33	0.050	:11.[b]			
Core	0.14	0.60	0.5	3.	—	313.6	0.00298	8.8	1.07		(0.6)
Bulge	0.96	2.4	0.6	3.	—	313.6	0.00298	5.3	1.01	0.70	0.73
Halo	:4.5	1.8	:0.55	:1.9	—	26.98	0.0625	:2.4	:0.70	(-0.2)	:0.46
Disk(+)	3.8	7.9	0.17	.6	0.66	1.868	0.986	15.	0.82	0.47	0.61
Flat(+)	:8.3	:0.72	:0.02	:0.52	:0.61	1.619	1.10	:2.0	:0.74	:-0.17	:0.76
Corona	:120.	400.	:1.	—	—	14.82	0.151	—	—	—	—

1. Colour indices in parenthesis are uncertain.
2. The parameters for the disk and flat subsystems are for positive mass components.
3. The parameters marked with a colon were kept fixed during the fitting process.
[a] The nucleus includes a point mass $2.65 \cdot 10^8$ $M_\odot$ at the centre.
[b] This is the mass-to-light ratio in V-colour.

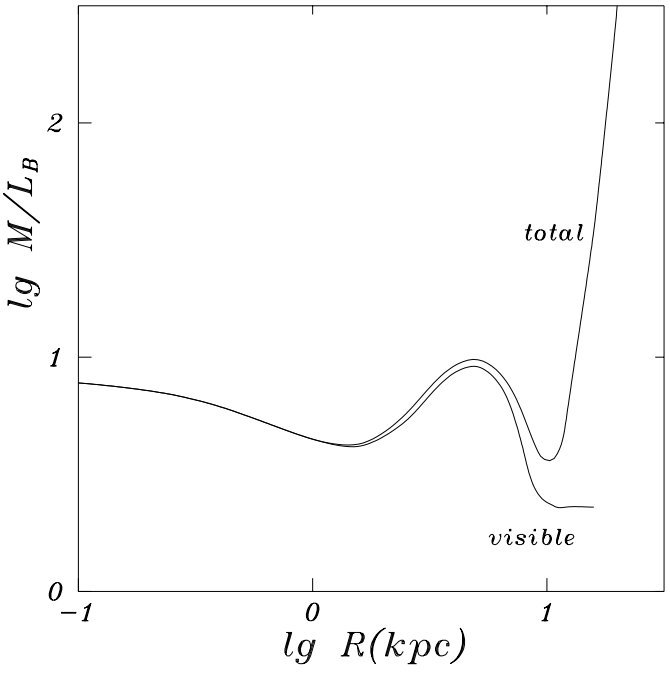

Fig. 13. Local mass-to-luminosity ratios for visible matter only and for visible + dark matter

of Brandt et al (1972) B-colour photometry and Rots (1975) HI velocities. The M/L_B ratio for the bulge was determined to lie between 5.6 and 11, for the disk between 10 and 14.

A different two-component model (Brandt spherical model for the bulge + exponential disk with a central hole) was constructed by Rohlfs & Kreitschmann (1980). As observational data they used the surface photometry from Brandt et al. (1972) and Schweizer (1976), the rotation velocities from Goad (1976), Rots (1975) and their own measurements. The structural parameters of the components were determined by fitting the model calculations with the observed rotation curve. The M/L ratios were derived by comparison with the light distribution in BV-colours along the major axis. Their model represents more adequately the observed rotational velocities for $R < 6$ kpc. The M/L_B derived from this model were between 3 and 20 for the bulge, between 6 and 11 for the disk.

Kent (1987) used his own r-colour photometry and rotation velocities measured by Rots (1975) and reprocessed by Visser (1980). In his model photometry along major and minor axis was used. The disk was assumed infinitely thin. Near the centre Kent decided not to use rotation velocities measured by Goad (1976) emphasizing that corrections for noncircular motions are very uncertain. For that reason the M/L for the bulge was also uncertain. For the disk $M/L_r = 3.7$ (corresponding to $M/L_B \simeq 4.8$).

When modelling the spiral structure of M 81 Lowe et al. (1994) constructed also a mass distribution model. They used the same observational data as Kent (central kinematics was interpreted slightly differently), but in addition also the morphology of spiral arms. The resulting M/L was the same for the bulge and the disk $M/L_r = 4.0$ (giving $M/L_B \simeq 5.2$).

It is seen that within the errors and especially when taking into account model differences all these values coincide with those of our model. We would like to point out two differences.

Firstly, difference in determining the mass of the spheroidal component. In our model the masses of the inner spheroid components (core and bulge) were determined mainly on the basis of the velocity dispersion data. In the models referred above the bulge mass was determined on the basis of the inner part of the rotation curve. Thus, the differences in calculated bulge M/L ratios are not surprising.

In studying the UV morphology of the central parts of M 81 (the core and the bulge in our notation) Reichen et al. (1995) noted variations in major axis position angle at $30'' < a < 50''$ ($0.5 < a < 0.9$ kpc). Thus it is possible that the core/bulge may have a triaxial symmetry. Together with noncircular motions it may explain why the observed rotational velocities at innermost points deviate from the model calculations. According to Devereux et al. (1995) the existence of shock waves can

Table 3. Calculated descriptive functions

R	K_R	$\log M(R)$							$f_{\rm B}$
(kpc)	$(\mathrm{km}^2/\mathrm{s}^2\mathrm{kpc})$	core	bulge	halo	disk	flat	corona	total	$(\mathrm{M}_\odot/\mathrm{L}_\odot)$
0.01	$1.41\ 10^7$	-2.65						-1.48	10.
0.02	$4.59\ 10^6$	-2.03						-1.37	8.8
0.04	2.88	-1.48	-2.57					-1.16	8.3
0.06	1.24	-1.20	-2.17					-0.98	8.1
0.08	$9.59\ 10^5$	-1.02	-1.90					-0.84	7.9
0.1	7.86	-0.89	-1.70					-0.74	7.7
0.2	4.12	-0.56	-1.12					-0.42	7.0
0.3	2.69	-0.42	-0.82	-2.60				-0.25	6.3
0.4	1.95	-0.35	-0.62	-2.29				-0.14	6.1
0.6	1.19	-0.28	-0.37	-1.88				0.00	5.3
0.8	$8.19\ 10^4$	-0.24	-0.22	-1.59				0.09	4.8
1.	6.05	-0.23	-0.10	-1.38			-2.91	0.15	4.5
2.	2.33	-0.22	0.16	-0.80			-2.03	0.34	4.5
2.5	1.81		0.22	-0.63	-1.83		-1.75	0.41	5.8
3.	1.50		0.27	-0.50	-0.52		-1.52	0.50	7.0
4.	1.25		0.31	-0.33	0.16		-1.15	0.67	8.8
5.	1.13		0.35	-0.20	0.41		-0.86	0.82	9.5
6.	1.00		0.36	-0.12	0.53	-2.68	-0.63	0.92	9.0
7.	$8.51\ 10^3$		0.37	-0.05	0.58	-1.30	-0.44	0.99	7.2
8.	7.08		0.38	0.00	0.60	-0.91	-0.28	1.02	5.6
9.	5.83			0.05	0.62	-0.67	-0.14	1.04	4.3
10.	4.88			0.07	0.63	-0.53	-0.01	1.06	3.6
13.	3.08			0.13	0.64	-0.39	0.29	1.08	8.3
16.	2.23			0.16		-0.35	0.51	1.12	35.
20.	1.66			0.18		-0.34	0.74	1.19	250.
23.	1.41						0.87	1.22	1200.
26.	1.23						0.98	1.29	
30.	1.08						1.11	1.35	
40.	$8.46\ 10^2$						1.34	1.50	
60.	6.08						1.62	1.71	

be used in explaining also specific Hα morphology and hot dust temperature in the bulge of M 81.

Secondly, our model includes a DM component – the corona (only the model by Lowe et al. (1994) includes also DM). On the basis of the rotation curve only it is not possible to determine all three free parameters of the DM distribution. Due to the limited extent of the rotation curve only the central density of the DM component can be determined. For this reason, we used additional data on the distribution and kinematics of satellite galaxies of M 81. Thus the DM distribution parameters are restricted with sufficient precision.

Our model gives for the mean line-of-sight velocity dispersion of globular clusters $\langle\sigma\rangle_{halo} = 130$ km/s. This is less than measured by Perelmuter et al. (1995) $\langle\sigma\rangle_{GC} = 150$ km/s. Because globular clusters lie in the gravitational potential of the whole galaxy, increasing of the mass of the halo or the mass of the DM corona within reasonable limits does not reduce the discrepancy significantly. In order to have the measured dispersion the mass within $R = 20$ kpc (outer extent of globular clusters population) must be $2.3 \cdot 10^{11}\,\mathrm{M}_\odot$. This mass gives the circular velocity at 20 kpc approximately 220 km/s. Such a high value is in conflict with the observed rotation curve. For this reason we were satisfied with the dispersion calculated from our model.

The model without DM component has the following deficiencies:

1. it is in conflict with the M 81 group velocity dispersion;
2. it is in conflict with the rotation curve for $R > 16$ kpc;
3. calculated velocity dispersion of globular clusters is 100 km/s which is in quite serious conflict with the measured value.

For this reason we conclude that the best fit with observational data is obtained in models which include a DM component.

Rather high axial ratio $\epsilon = 0.17$ may indicate that our old disk is a mixture of an old thin disk and a thick disk (see Wyse & Gilmore 1995). Indirect argument for the presence of a thick disk is also the chemical composition gradient of HII regions measured by Henry & Howard (1995). Unfortunately, in this study we cannot give pro or contra arguments about the thick disk in M 81.

Finally, we would like to discuss the nucleus. The mass of the nucleus was determined on the basis of the velocity dispersion 250 km/s measured by Bower et al. (1996) (see Sect. 3.1). The point mass in the centre of our model has $M_{BH} = 2.7 \cdot 10^8\,\mathrm{M}_\odot$, corresponding to the $M/L_V = 11\,\mathrm{M}_\odot/\mathrm{L}_\odot$ of the stellar nucleus. This BH mass is significantly larger than it was estimated by Ho et al. (1996) $\sim 3 \cdot 10^6\,\mathrm{M}_\odot$. In principle, these dispersion measurements may be handled as being only preliminary results. However, even when we accept the 'standard' M 81 central velocity dispersion (McElroy 1995) 170 km/s within $1''$ the M/L ratio of the stellar nucleus, corresponding to the point mass $3 \cdot 10^6\,\mathrm{M}_\odot$, is $M/L_V \simeq 50\,\mathrm{M}_\odot/\mathrm{L}_\odot$. This value also disagrees with M/L resulting from chemical evolution models of stellar populations and, we rejected it. Thus we decided in our final model to start with $M_{BH} = 2.7 \cdot 10^8\,\mathrm{M}_\odot$. The BH mass in our model is in quite good agreement with the general trend of BH mass versus luminosity of the spheroid (Ford et al. 1998).

Acknowledgements. We would like to thank the referee, Nicola Caon, for useful comments. This work was partially supported by the Estonian Science Foundation through grants 180 and 2627.

Appendix A: model construction

We assume a galaxy to consist of several physically homogeneous components with masses M, mass-to-light ratios f and fixed colour indices. In order to fit model parameters *simultaneously* by using both photometrical data and kinematical data more practical is to start with sufficiently flexible spatial density distribution $\rho(a)$. Otherwise we need to calculate the observable dynamical functions (rotational velocities and velocity dispersions) of the model via the surface density distribution, which is more complicated. The density distribution of each component we approximated as an inhomogeneous ellipsoid of rotation with a constant axial ratio $\epsilon = b/a$. All components, except the corona, form an optically visible part of the galaxy, and their volume densities are described by a modified exponential law

$$\rho(a) = \rho(0)\exp(-[a/(ka_0)]^{1/N}), \qquad (A1)$$

allowing a description of both the light profiles of disks and of spheroidal components by simply varying the structure parameter N. Similar density distribution law for surface densities was introduced by Sersic (1968) and independently for spatial densities by Einasto (1969b). This is a simple law allowing sufficiently precise numerical integration and has a minimum number of free parameters (two scale parameters and a density gradient parameter). The remaining component – the invisible massive corona – is represented by a modified isothermal law

$$\rho(a) = \begin{cases} \rho(0)([1+(\frac{a}{a_c})^2]^{-1} - [1+(\frac{a^0}{a_c})^2]^{-1}) & a \le a^0 \\ 0 & a > a^0. \end{cases} \qquad (A2)$$

In these formulae $\rho(0) = hM/(4\pi\epsilon {a_0}^3)$ is the central density, a is the distance along the major axis, $a_c = ka_0$ – the core radius, a_0 – the harmonic mean radius, a^0 – the outer cutoff radius for the corona, and h and k are normalizing parameters, depending on the parameter N (Paper IV, Appendix B).

For the disk and the flat components we use the density distribution in the following form

$$\rho(a) = \rho_+(a) + \rho_-(a), \qquad (A3)$$

where subindices "–" and "+" denote density distributions (1) with negative and positive masses, respectively. In this way we have density distributions with central density depression. If we demand that the density is zero at $a = 0$ and positive elsewhere, the following relations must hold between the parameters of components ρ_+ and ρ_- : $a_{o-} = \kappa a_{o+}$, $M_- = -\kappa^2 M_+$, $\epsilon_- = \epsilon_+/\kappa$, where $\kappa < 1$ is a parameter which determines the relative size of the hole in the centre of the disk. The structural parameters N_- and N_+ were assumed to be equal.

The density distributions for visible components were projected along the line of sight and their superposition gives us the surface brightness distribution of the model

$$L(A) = 2\sum_i^n \frac{\epsilon_i}{E_i f_i} \int_A^\infty \frac{\rho_i(a)a\,da}{(a^2 - A^2)^{1/2}}, \qquad (A4)$$

where A is the major semiaxis of the equidensity ellipse of the projected light distribution, n is the number of components and E_i are their apparent axial ratios.

The masses of the components can be determined from the rotation law

$$v_i^2(R) = 4\pi\epsilon_i G \int_0^R \frac{\rho_i(a)a^2 da}{(R^2 - e_i^2 a^2)^{1/2}}, \qquad (A5)$$

$$V^2(R) = \sum_i^n v_i^2(R). \qquad (A6)$$

where G is the gravitational constant and R is the distance in the equatorial plane of the galaxy.

For "hot" components the masses were determined from the virial theorem for multicomponent systems connecting the mean line-of-sight velocity dispersion of the k-th component with the masses of all components M_l (q.v. Paper IV, Appendix A)

$$\langle\sigma^2\rangle_k = \frac{G}{a_{0k}} \sum_{l=1}^m H_{kl} M_l. \qquad (A7)$$

In this formula m is the total number of components and H_{kl} are dimensionless coefficients depending on the mass distribution laws (parameter N) of the components k and l. It is evident that all subsystems contribute to the mean velocity dispersion of a particular component, but often the influence of the component $k = l$ is more or less dominating.

For a point mass within a spherical stellar nucleus the virial theorem for multicomponent systems has a form

$$\langle\sigma^2_{nucl}\rangle = \frac{G}{3a_0}\left(M_{BH} + \gamma M_{nucl}\right), \qquad (A8)$$

where parameter γ depends on the structure parameter N of the nucleus and M is mass.

References

Adler, D.S., Westphal, D.J., 1996, AJ 111, 735
Allen, R.J., Knapen, J.H., Bohlin, R., Stecher, T.P., 1997, ApJ 487, 171
Appleton, P.N., Davies, R.D., Stephenson, R.J., 1981, MNRAS 195, 327
Bender, R., Saglia, R.P., Gerhard, O.E., 1994, MNRAS 269, 785
Bietenholz, M.F., Bartel, N., Rupen, M.P., et al., 1996, ApJ 457, 604
Blandford, R.D., Narayan, R., 1992, ARA&A 30, 311
Bower, G.A., Wilson, A.S., Heckman, T.M., Richstone, D.O., 1996, AJ 111, 1901
Brandt, J.C., Kalinowski, J.K., Roosen, R.G., 1972, ApJS 24, 421
Bressan, A., Chiosi, C., Fagotto, F., 1994, ApJS 94, 63
Brouillet, N., Baudry, A., Combes, F., 1988, A&A 196, L17
Brouillet, N., Baudry, A., Combes, F., Kaufman, M., Bash F., 1991, A&A 242, 35
Burstein, D., Heiles, C., 1984, ApJS 54, 33
Capaccioli, M., Caon, N., 1992, in: Morphological and Physical Classification of Galaxies, Longo G., Capaccioli M., Busarello G. (eds.), Kluwer, Dordrecht, p. 99
Carter, D., Jenkins, C.R., 1993, MNRAS 263, 1047
Cohen, J.G., 1979, ApJ 228, 405
Crane, P., Stiavelli, M., King, I.R. et al., 1993, AJ 106, 1371
de Jong, R.S., 1996, A&A 313, 45
Davidge, T.J., 1997, AJ 113, 985
Delisle, S., Hardy, E., 1992, AJ 103, 711
Devereux, N.A., Jacoby, G., Ciardullo, R., 1995, AJ 110, 1115
Devereux, N., Ford, H., Jacoby, G., 1997, ApJ 481, L71
Einasto, J., 1967a, Tartu Astr. Obs. Publ. 36, 357
Einasto, J., 1967b, Tartu Astr. Obs. Publ. 36, 442
Einasto, J., 1969a, Astr. Nachr. 291, 97
Einasto, J., 1969b, Astrofizika 5, 137
Einasto, J., 1970, Tartu Astr. Obs. Teated 26, 1
Einasto, J., 1972, Tartu Astr. Obs. Teated 40, 3; also in: Stars and the Milky Way System, Proc. First European Ast. Meet. vol 2, Mavridis L.N. (ed.), Springer, Berlin, Heidelberg, New York, p. 291
Einasto, J., Einasto, L., 1972a, Tartu Astr. Obs. Teated 36, 3
Einasto, J., Einasto, L., 1972b, Tartu Astr. Obs. Teated 36, 46
Einasto, J., Haud, U., 1989, A&A 223, 89 (Paper I)
Einasto, J., Rümmel, U., 1972, Tartu Astr. Obs. Teated 36, 55
Einasto, J., Tenjes, P., Barabanov, A.V., Zasov, A.V., 1980a, Ap&SS 67, 31
Einasto, J., Tenjes, P., Traat, P., 1980b, Astron. Circ. No.1089, 1
Elmegreen, D.M., Elmegreen, B.G., 1984, ApJS 54, 127
Elson, R.A.W., Santiago, B.X., 1996, MNRAS 278, 617
Fabbiano, G., 1989, ARA&A 27, 87
Ford, H.C., Tsvetanov, Z.I., Ferrarese, L., Jaffe, W., 1998, in: The central regions of the Galaxy and galaxies. Proc. IAU Symp 184, Kyoto 1997, = astro-ph/9711299
Fort, B., Mellier, Y., 1994, A&AR 5, 239
Freedman, W.L., Hughes, S.M., Madore, B.F. et al., 1994, ApJ 427, 628
Freeman, K.C., 1993, in "Physics of nearby galaxies: nature or nuture?", eds. T.X. Thuan, C. Balkowski & J.T. Thanh Van, Editions Frontières, p. 201
Garcia-Gomez, C., Athanassoula, E., 1991, A&AS 89, 159
Georgiev, Ts.B., Getov, R.G., 1991, Pisma v AZh 17, 393
Georgiev, Ts.B., Tikhonov, N.A., Karachentsev, I.D., 1991a, SvA Lett. 17, 165
Georgiev, Ts.B., Tikhonov, N.A., Karachentsev, I.D., 1991b, SvA Lett. 17, 416
Gilmore, G., King, I., van der Kruit, P., 1990, The Milky Way as a galaxy, Geneva Observatory: Sauverny-Versoix, Switzerland, Chapter 11
Gilmore, G., Wyse, R.F.G., Jones, J.B., 1995, AJ 109, 1095
Goad, J.W., 1976, ApJS 32, 89
Gottesman, S.T., Weliachew, L., 1975, ApJ 195, 23
Guidoni, U., Messi, R., Natali, G., 1981, A&A 96, 215
Haud, U., 1985, PhD Thesis, Tartu Astr. Obs.
Haud, U., Einasto, J., 1989, A&A 223, 59
Henry, R.B.C., Howard, J.W., 1995, ApJ 438, 170
Hill, J.K., Cheng, K.-P., Bohlin, R.C. et al., 1995, ApJ 438, 181
Ho, L.C., Filippenko, A.V., Sargent, W.L.W., 1996, ApJ 462, 183
Hodge, P.W., 1989, ARA&A 27, 139
Hodge, P.W., Kennicutt, Jr. R.C., 1983, AJ 88, 296
Högner, W., Kadla, Z., Richter, N., Strugatskaja, A., 1971, Afz 7, 407
Huchtmeier, W.K., Skillman, E.D., 1995, in: Richter O.-G., Borne K. (eds.) Groups of galaxies, ASP Conference Series, Vol. 70, ASP: California, U.S.A., p. 155
Illingworth, G., 1980, in: ESO workshop on two-dimensional photometry, Crane P., Kjär K. (eds.). ESO, p. 299
Ivanov, G.R., 1992, MNRAS 257, 119
Keel, W.C., 1989, AJ 98, 195
Kent, S.M., 1987, AJ 93, 816
Kormendy, J., 1985, ApJ 292, L9
Lowe, S.A., Roberts, W.W., Yang, J., Bertin, G., Lin, C.C., 1994, ApJ 427, 184
Majewski, S.R., 1993, ARA&A 31, 575
Markaryan, B.E., Oganesyan, E.Y., Arakelyan, S.N., 1962, Soobshch. Byurakan. Obs. 30, 3
McElroy, D.B., 1995, ApJS 100, 105
Méra, D., Chabrier, G., Schaeffer, R., 1998, A&A (in press) = astro-ph/9801050
Mihalas, D., Binney, J., 1981, Galactic astronomy: structure and kinematics, 2nd ed., Freeman: San Francisco
Monnet, G., Simien, F., 1977, A&A 56, 1973
Morrison, H.L., Harding, P., 1993, PASP 105, 977
Ng, Y.K., Bertelli, G., Chiosi, C., Bressan, A., 1997, A&A 324, 65
O'Connell, R.W., Bohlin, R.C., Collins, N.R., et al., 1992, ApJ 395, L45
Perelmuter, J.-M., Racine, R., 1995, AJ 109, 1055
Perelmuter, J.-M., Brodie, J.P., Huchra, J.P., 1995, AJ 110, 620
Petit, H., Sivan, J.-P., Karachentsev, I.D., 1988, A&AS 74, 475
Prieto, M., Beckman, J.E., Cepa, J., Varela, A.M., 1992, A&A 257, 85
Pryor, C., Meylan, G., 1993, in: Djorgovski S.G., Meylan G. (eds.) Structure and dynamics of globular clusters, ASP Conf. Ser. Vol. 50, ASP: San Francisco, U.S.A., p. 357
Racine, R., 1991, AJ 101, 865
Reed, L.G., Harris, G.L.H., Harris, W.E., 1994, AJ 107, 555
Reichen, M., Kaufman, M., Blecha, A., Golay, M., Huguenin, D., 1994, A&AS 106, 523
Roberts, M.S., Rots, A.H., 1973, A&A 26, 483
Rohlfs, K., Kreitschmann, J., 1980, A&A 87, 175
Rohlfs, K., Kreitschmann, J., 1988, A&A 201, 51
Rose, J., 1985, AJ 90, 1927
Rots, A.H., 1975, A&A 45, 43
Sage, L.J., Westphal, D.J., 1991, A&A 242, 371
Sandage, A.R., Becklin, E.E., Neugebauer, G., 1969, ApJ 157, 55
Schweizer, F., 1976, ApJS 31, 313
Secker, J., Geisler, D., McLaughlin, D.E., Harris, W.E., 1995, AJ 109, 1019
Sersic, J.L., 1968, Atlas de Galaxies Australes, Observatorio Astronomico, Cordoba, Argentina

Shaw, M.A., Gilmore, G., 1990, MNRAS 242, 59
Simien, F., 1988, in: The world of galaxies, Corwin Jr., H.G., Bottinelli L. (eds.). Springer: New York, p. 293
Simkin, S.M., 1967, AJ 72, 1032
Tenjes, P., 1992, Baltic Astronomy 1, 7
Tenjes, P., Einasto, J., Haud, U., 1991, A&A 248, 395 (Paper III)
Tenjes, P., Haud, U., Einasto, J., 1994, A&A 286, 753 (Paper IV)
van den Bergh, S., 1975, ARA&A 13, 217
van der Kruit, P.C., Gilmore, G. (Eds.), 1995, Stellar populations, Proc. 164th Symposium of the IAU, Aug. 15–19, 1994, The Hague, The Netherlands. Kluwer Academic Publishers: Dordrecht, Boston, London
van Driel, W., Kraan-Korteweg, R.C., Binggeli, B., Huchtmeier, W.K., 1998, A&AS 127, 397
Visser, H.C.D., 1980, A&A 88, 149
Worthey, G., 1994, ApJS 95, 107
Wyse, R.F.G., Gilmore, G., 1995, AJ 110, 2771
Yun, M.S., Ho, P.T.P., Lo, K.Y., 1994, Nature 372, 530
Zepf, S.E., Ashman, K.M., Geisler, D., 1995, ApJ 443, 570